Regionale Ozeanographie

12 – Indischer Ozean

Pergamon

Progress in Oceanography 51 (2001) 1–123

Progress in Oceanography

www.elsevier.com/locate/pocean

The monsoon circulation of the Indian Ocean

Friedrich A. Schott [a,*], Julian P. McCreary Jr. [b]

[a] Institut für Meereskunde an der Universität Kiel, Kiel, Germany
[b] International Pacific Research Center, University of Hawaii, Honolulu, Hawaii, USA

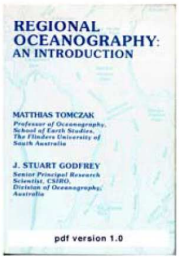

http://www.cmima.csic.es/mirror/mattom/regoc/pdfversion.html

Global Ocean Bathymetry

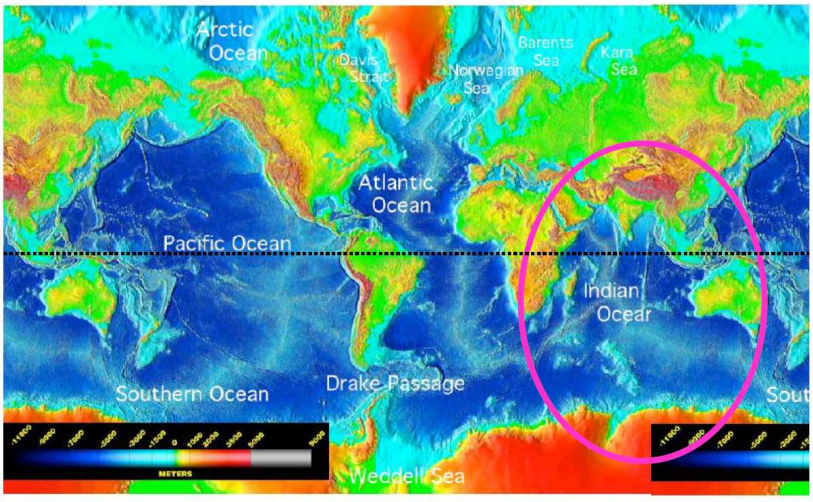

Indian Ocean bathymetry

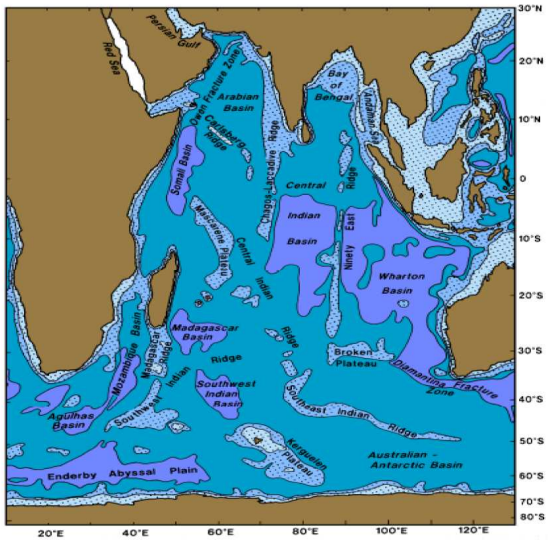

Tomczak & Godfrey, 2005

Global SST and SSS

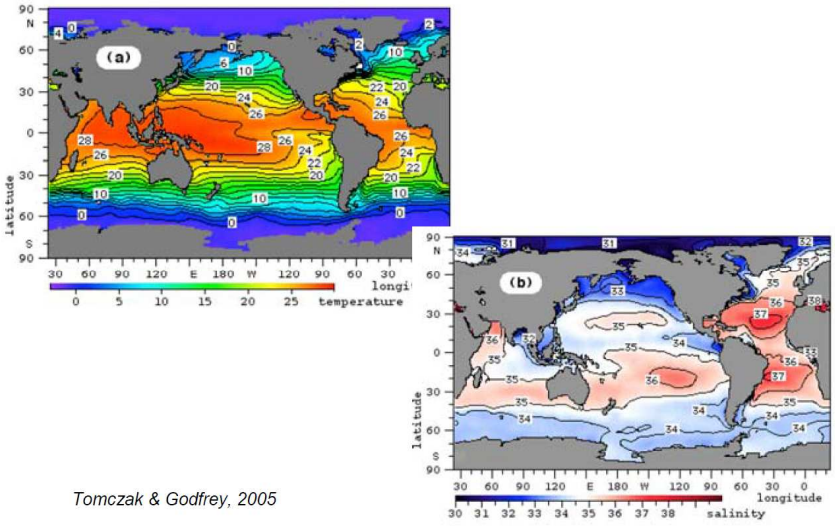

Tomczak & Godfrey, 2005

Global SL Pressure and winds

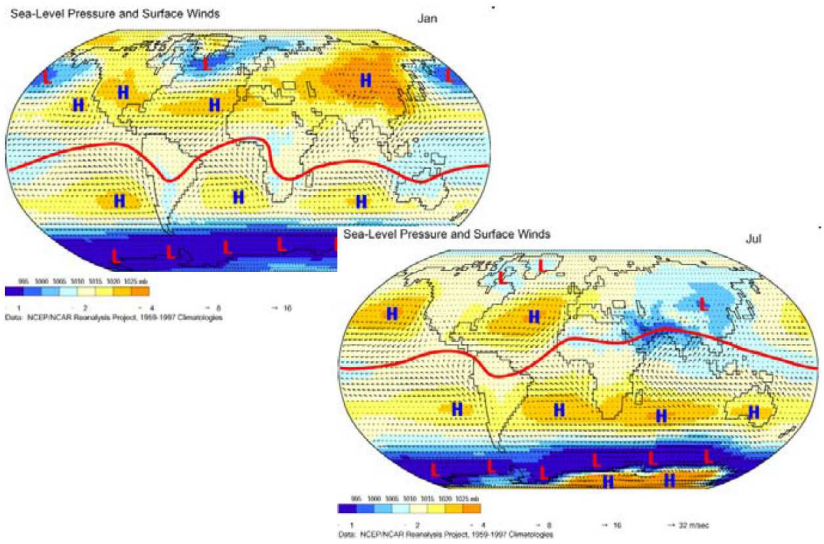

Monsoon winds – northern Indian Ocean

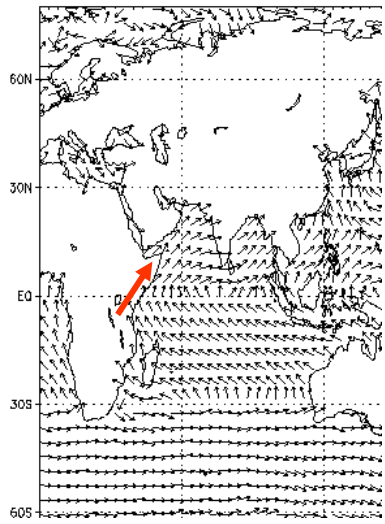

SW monsoon winds

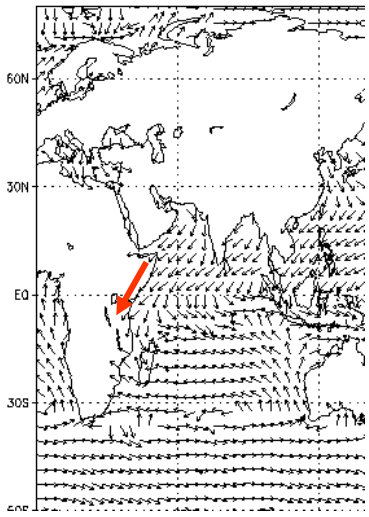

NE monsoon winds

IO – seasonal wind

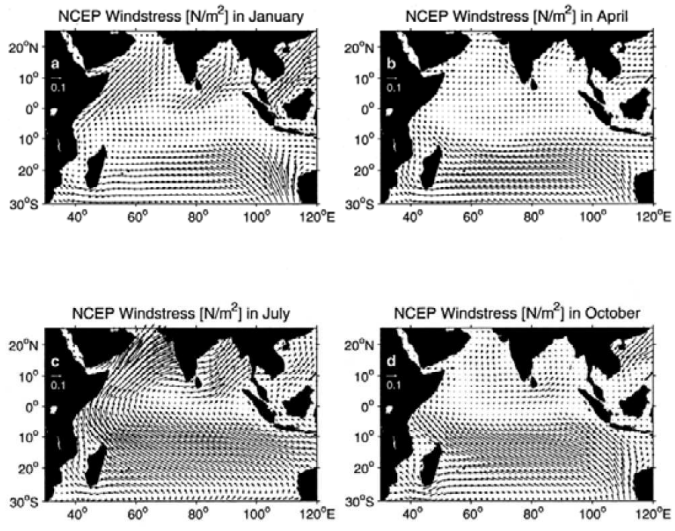

Fig. 1. Monsoon wind stress fields from the NCEP climatology for a) January; b) April; c) July; d) November.

Schott & McCreary, 2001

Wind-driven circulation

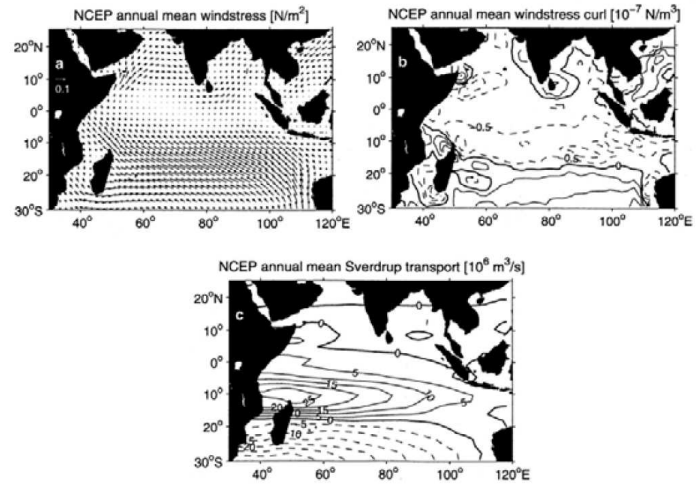

Fig. 4. Annual mean fields of a) wind stress; b) wind stress curl; c) Sverdrup transport function (in Sv=10^6 m^3 s^{-1}), from NCEP climatology.

Schott & McCreary, 2001

Sea surface temperature

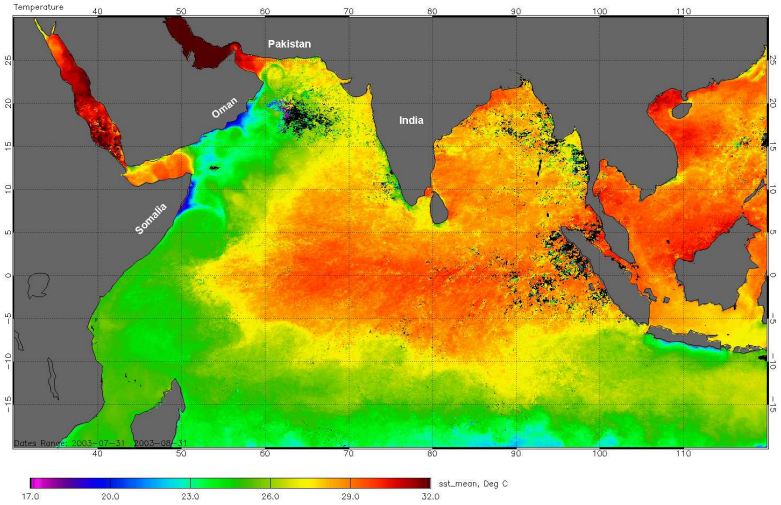

July 2003 SST: Low along Somalia and Arabian peninsula during SW monsoon. (NASA MODIS satellite, NASA GSFC)

Talley et al., 2010

Upwelling

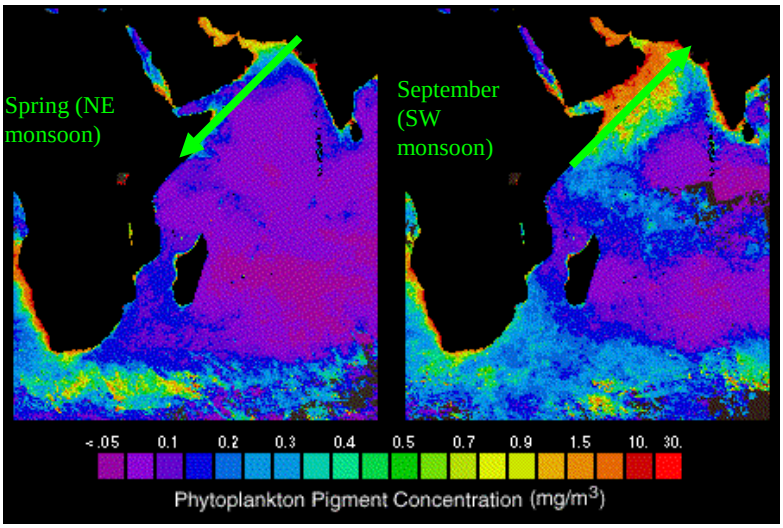

Talley et al., 2010

Near surface circulation SW-Monsoon

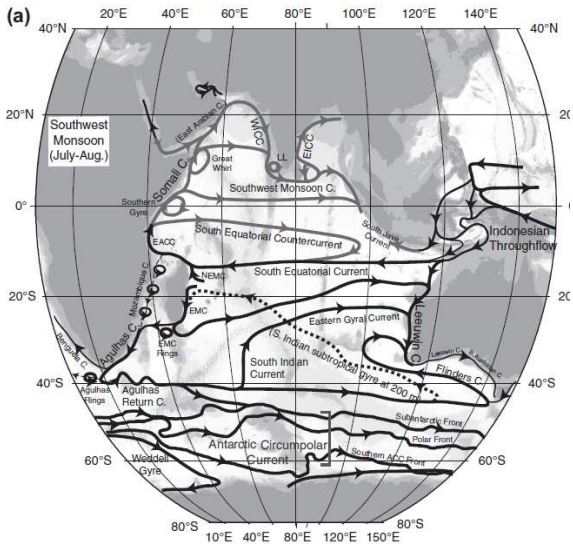

Talley at al., 2011

Near surface circulation SW-Monsoon

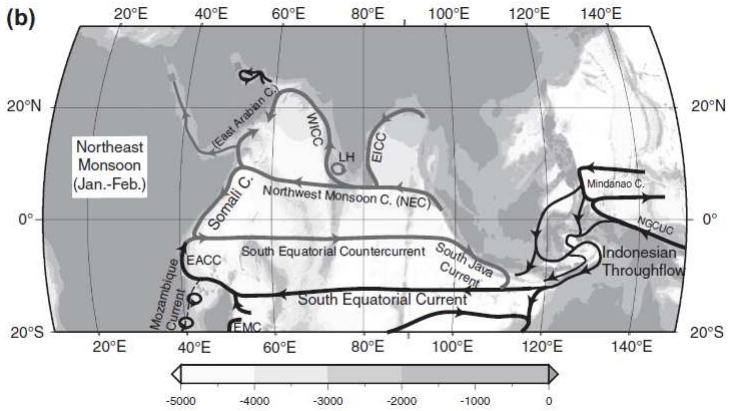

Talley at al., 2011

Salinity western IO

Arctic Intermediate Water

North Atlantic Deep W.

Antarctic Bottom Water

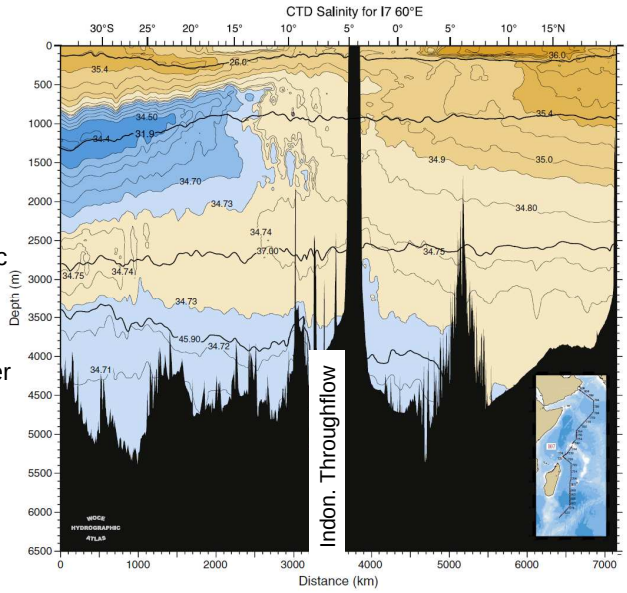

Persian Gulf Water

Red Sea Water

North Indian Deep Water

External water masses

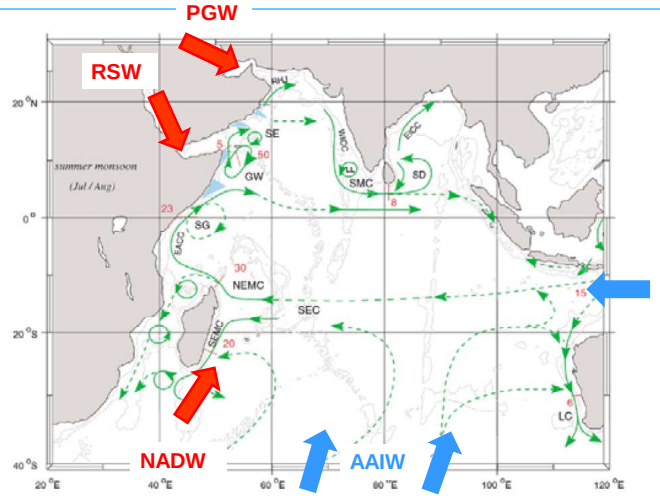

Fig. 8. A schematic representation of identified current branches during the Southwest Monsoon, including some choke point transport numbers (Sv=$10^6 m^3 s^{-1}$). Current branches indicated (see also Fig. 9) are the South Equatorial Current (SEC), South Equatorial Countercurrent (SECC), Northeast and Southeast Madagascar Current (NEMC and SEMC), East African Coast Current (EACC), Somali Current (SC), Southern Gyre (SG) and Great Whirl (GW) and associated upwelling wedges, Socotra Eddy (SE), Ras al Hadd Jet (RHJ) and upwelling wedges off Oman, West Indian Coast Current (WICC), Laccadive High and Low (LH and LL), East Indian Coast Current (EICC), Southwest and Northeast Monsoon Current (SMC and NMC), South Java Current (JC) and Leeuwin Current (LC). See text for details.

Schott & McCreary, 2001

Salinity western IO

Arctic Intermediate Water

North Atlantic Deep W.

Antarctic Bottom Water

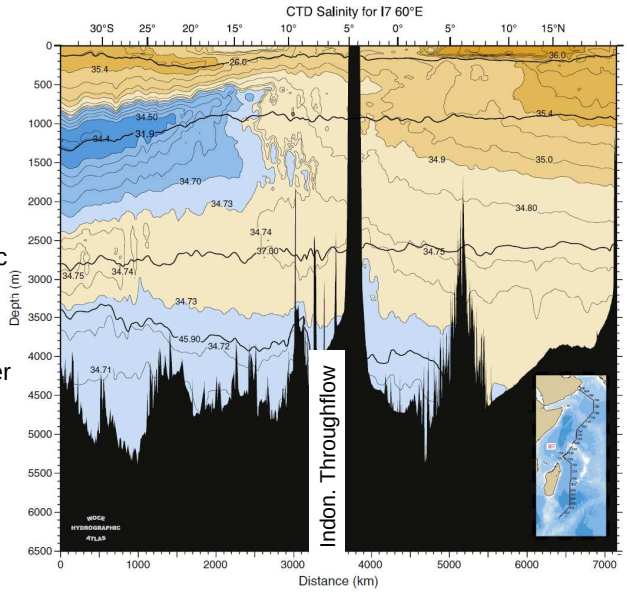

Persian Gulf Water

Red Sea Water

North Indian Deep Water

Freshwater Input Bay of Bengal

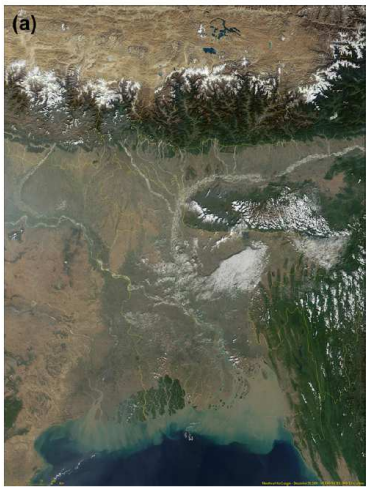

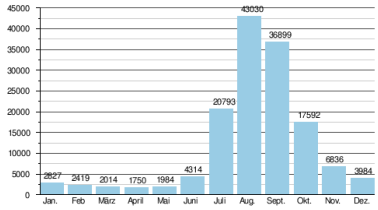

Ganges – Brahmaputra Delta

sea surface salinity

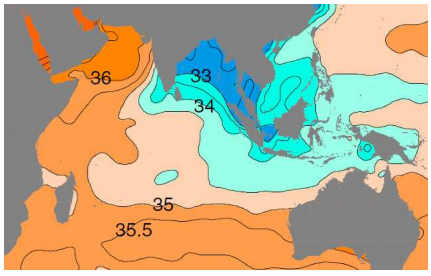

Arabian Sea – Bay of Bengal

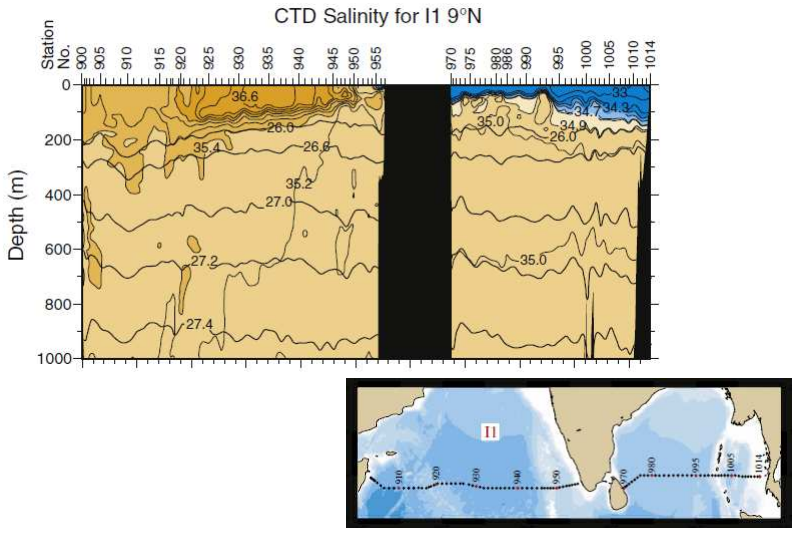

Water masses

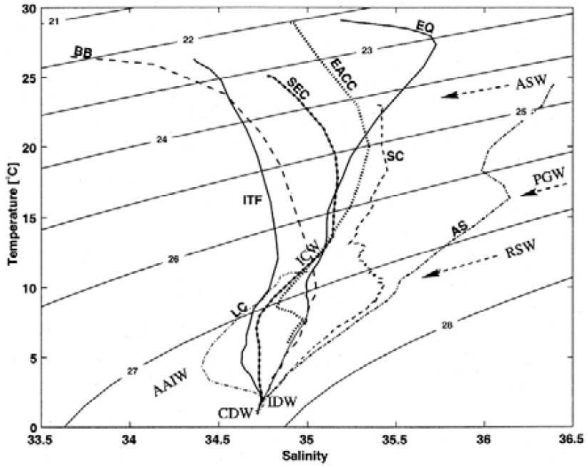

Fig. 7. Temperature-Salinity diagram of Indian Ocean water masses taken from Levitus and Boyer (1994a,b) climatology for the Bay of Bengal (BB), northern Arabian Sea (AS), equatorial region of western basin (EQ), South Equatorial Current (SEC), western exit of Indonesian Throughflow (ITF), and Leeuwin Current (LC). The Somali Current (SC) curve is from August 1993 measurements in northern upwelling wedge. Core water masses indicated are Circumpolar Deep Water (CDW), Indian Deep Water (IDW), Antarctic Intermediate Water (AAIW), Indian Central Water (ICW), Red Sea Water (RSW), Persian Gulf Water (PGW), and Arabian Sea Water (ASW). Profiles are for respective winter seasons in each hemisphere.

Schott & McCreary, 2001

Water masses thermocline

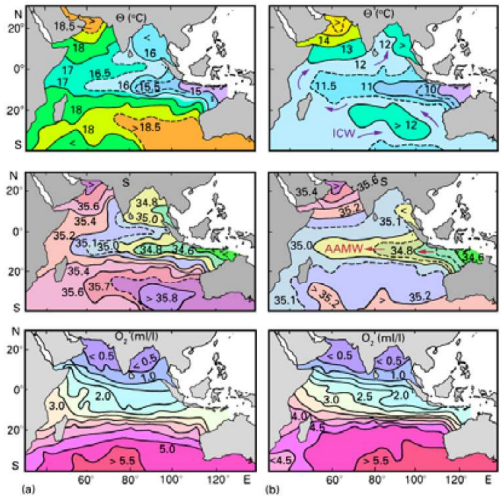

Fig. 12.9. Annual mean temperature (°C), salinity, and oxygen (ml/l) in the thermocline on isopycnal surfaces. (a) On the σ_Θ surface 25.7, located in the depth range 150 - 200 m, (b) on the σ_Θ surface 26.7, located in the depth range 300 - 450 m. Arrows indicate the movement of ICW and AAMW. After You and Tomczak (1993)

Tomczak & Godfrey, 2005

'Unusual' current systems

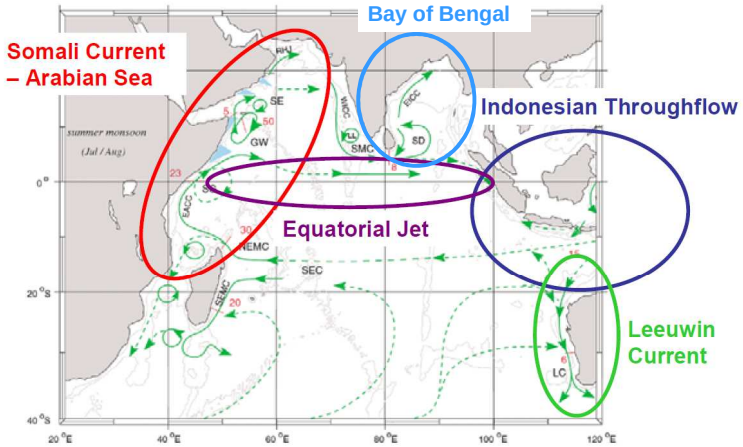

Fig. 8. A schematic representation of identified current branches during the Southwest Monsoon, including some choke point transport numbers (Sv=$10^6 m^3 s^{-1}$). Current branches indicated (see also Fig. 9) are the South Equatorial Current (SEC), South Equatorial Countercurrent (SECC), Northeast and Southeast Madagascar Current (NEMC and SEMC), East African Coast Current (EACC), Somali Current (SC), Southern Gyre (SG) and Great Whirl (GW) and associated upwelling wedges, Socotra Eddy (SE), Ras al Hadd Jet (RHJ) and upwelling wedges off Oman, West Indian Coast Current (WICC), Laccadive High and Low (LH and LL), East Indian Coast Current (EICC), Southwest and Northeast Monsoon Current (SMC and NMC), South Java Current (JC) and Leeuwin Current (LC). See text for details.

Schott & McCreary, 2001

Oberflächenströmungen Arabische See

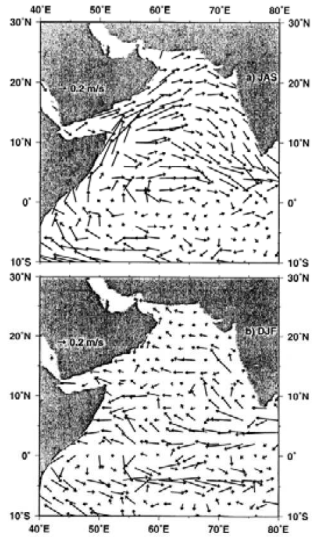

Somalistrom:

Frühere Erklärungen
Wind – Ekman Transport von der Küste weg – Aufbau eines barotropen Druckgradienten – küstenparallele geostrophische Strömung

Zeitskala: Mehrere Tage bis Wochen

Schott & McCreary, 2001

Fig. 31. Surface current vectors from drifter climatology for a) July–September; and b) December–February. (Courtesy A. Mariano.)

Somali Current

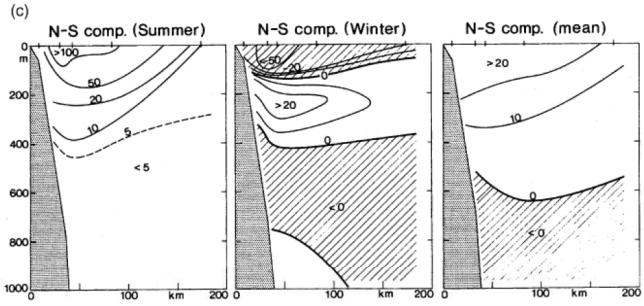

Fig. 33. Mean velocity sections across Indian Ocean western boundary currents for ~~a) Northeast Madagascar Current at Cape Amber (westward is positive), b) Southeast Madagascar Current at 23°S (southward is positive), both from Swallow et al. (1988), and~~ c) Somali Current on the equator (northward is positive) during the summer monsoon (left), during the winter monsoon (middle) and annual mean (right; from Schott et al., 1990); section locations see Fig. 20.

Schott & McCreary, 2001

Somali Current Upwelling

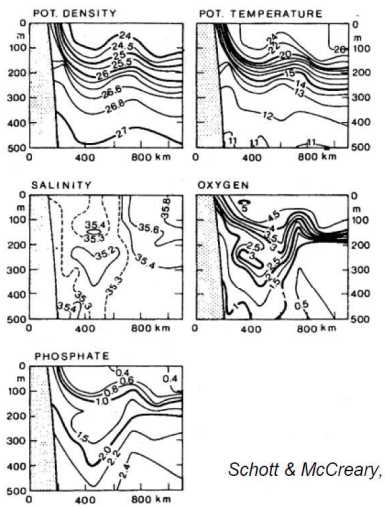

Schott & McCreary, 2001

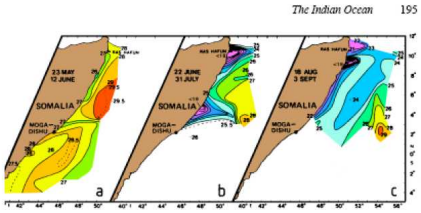

The Indian Ocean 195

11.16. Development of the Somali Current during the onset of the Southwest Monsoon as i in the sea surface temperature during 1979. (a) Advection of warm water south of 3°N and stal upwelling north of 3°N, (b) two gyres with upwelling regions near 4°N (minimum perature <19°C) and Ras Hafun (minimum temperature <18°C), (c) continuous northward flow upwelling near Ras Hafun (minimum temperature <17°C). From Evans and Brown (1981).

Tomczak & Godfrey, 2005

Fig. 37. Section along approx. 12°N through the northern Somali Current upwelling regime taken 29 August–1 September 1964 during a particularly strong upwelling episode, showing potential density (kg/m^3), potential temperature, salinity, oxygen (ml l^{-1}) and phosphate (μgatl^{-1}). (After Swallow & Bruce, 1966; see Fig. 20 for section location.)

Arabian Sea Upwelling

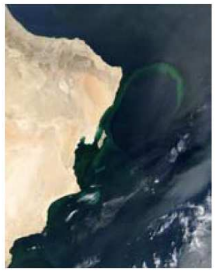

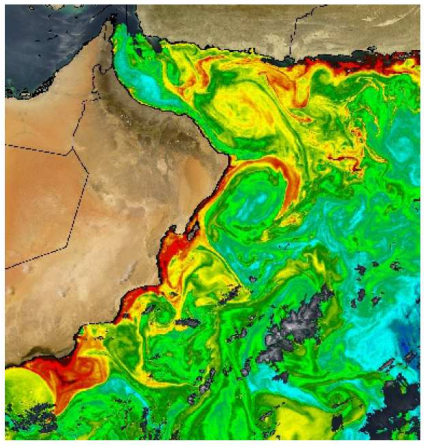

Energetic jets emerging from the coastal upwelling region cool the Arabian Sea and carry nutrients and other matter from the coastal region into the interior.

Indian Ocean Expedition 1960s

FS METEOR cruise 1964/65

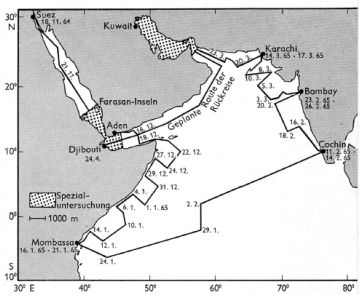

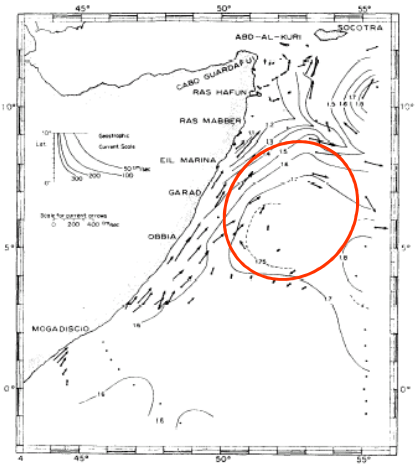

Seasonal reversal of the Somali Current

Great Whirl during summer monsoon

Swallow and Bruce, 1966

Somali Current at the equator

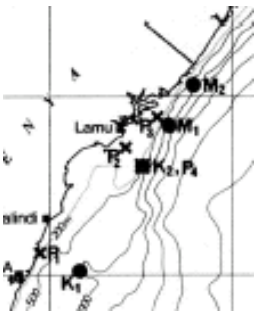

Response to the onset of the summer monsoon

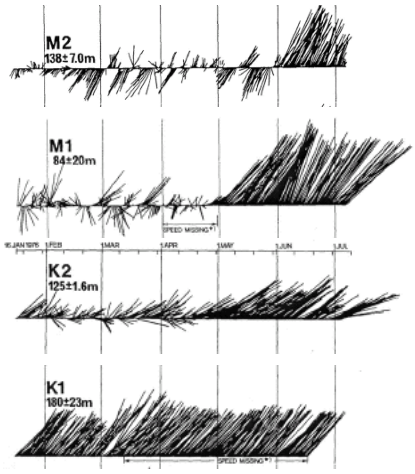

Düing and Schott, 1978

INDEX 1979

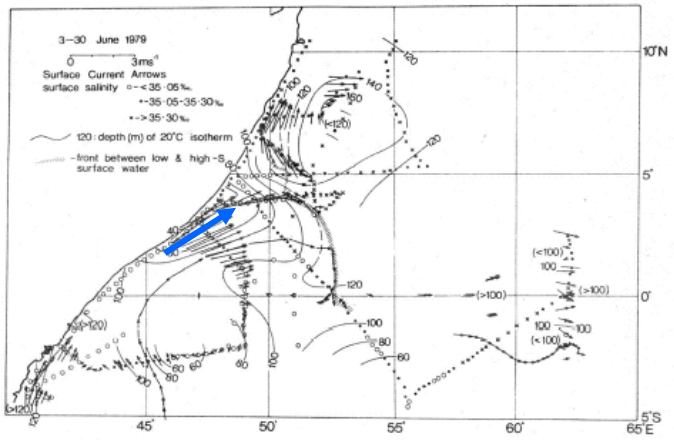

Development of the Somali Current in a two-gyre system

Evidence for remote forcing

Swallow et al., 1987

Big signal: > 7 kn

Somali Current

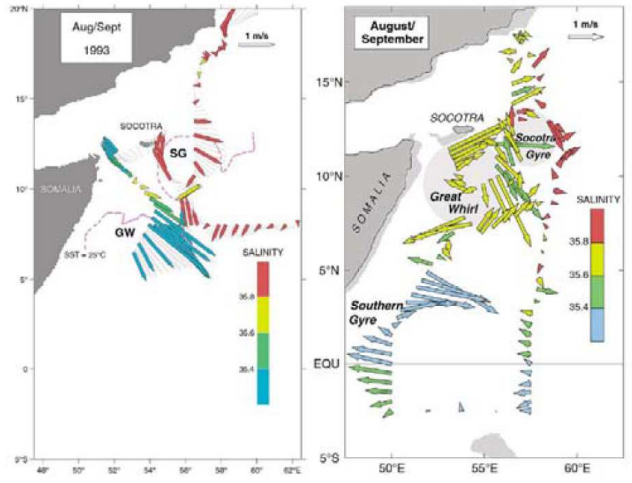

Fig. 36. Somali Current flow patterns during the late summer monsoon phases of a) 1993 (after Fischer et al., 1996) and b) 1995, (after Schott et al., 1997). Marked are the Southern Gyre, Great Whirl and Socotra Gyre. Near-surface salinities (colour-coded on the current vectors) indicate that lower-salinity waters originating from the southwestern and upwelling regions recirculate in the Great Whirl and do not leave the Somali Current zone toward the east in the 4°–12°N latitude belt. Instead, outflow from the northern Somali Current during the summer monsoon occurs through the Socotra Passage. Note also that the GW in 1995 was located much more northerly, against the banks of southern Socotra, than in 1993.

Schott & McCreary, 2001

Response Somalistrom – INDEX 1979

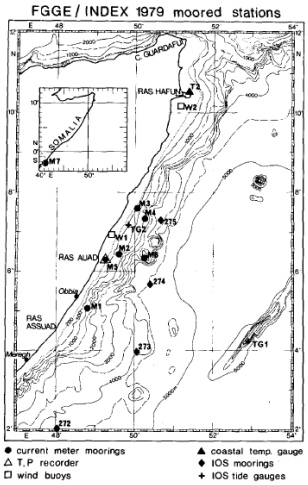

FIG. 1. Positions of moored instrumentation during INDEX from March to July, 1979. Depths in meters.

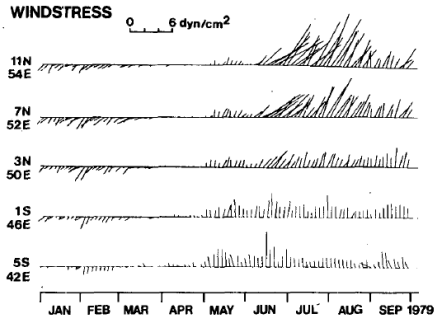

FIG. 3. Wind-stress vectors as determined from standard ship observations (Schott and Fernandez-Partagas, 1981) for five points along the East African coast during January to September, 1979; north is upward.

Schott & Quadfasel, 1982

Response Somalistrom

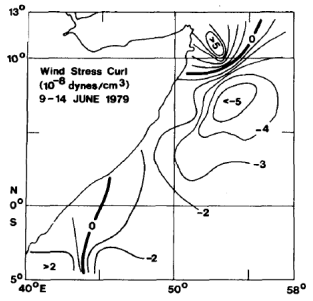

FIG. 12. Wind-stress curl off Somalia at time of final onset of summer monsoon, 9–14 June 1979.

Schott & Quadfasel, 1982

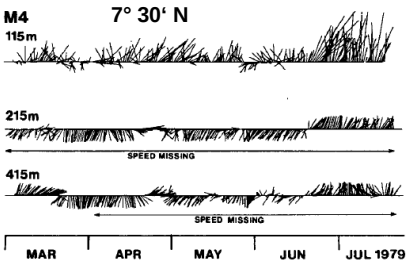

FIG. 4. (*Continued*)

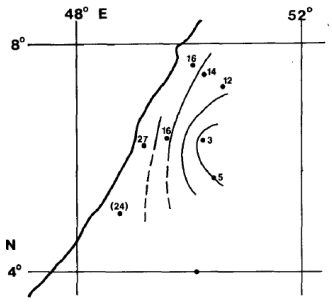

FIG. 8. Response time of currents at instruments of different moorings counted in days after final monsoon onset on 10 June 1979.

Response Somalistrom – WOCE 1995-96

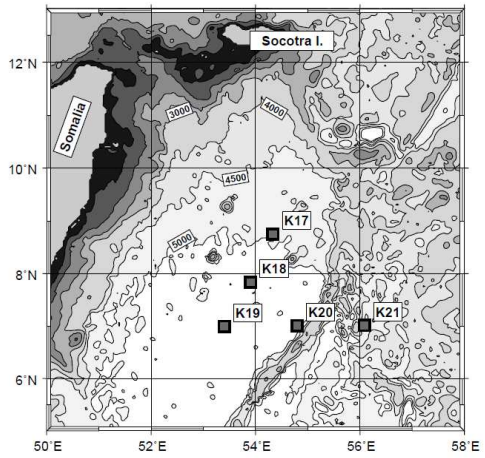

Verankerungsarray zum Testen des Wellenansatzes

Brandt et al., 2002

Somalistrom Wellenausbreitung

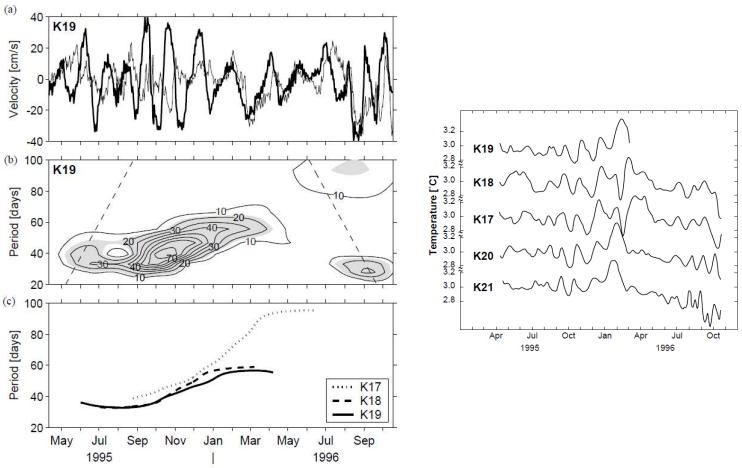

Fig. 8. (a) Time-series of zonal (thin solid line) and meridional (thick solid line) velocity at 400 m depth at mooring K19, (b) period–time plot of normalized meridional velocity wavelet energy at 400 m depth at mooring K19, and (c) periods of maximum oscillation amplitude at 400 m depth at the three moorings K17–K19. The light gray shaded areas in (b) mark the regions with a significance level higher than 95%. The curves shown in (c) are plotted only in these regions. The locations of the moorings are given in Fig. 1.

Brandt et al., 2002

Somalistrom Wellenausbreitung

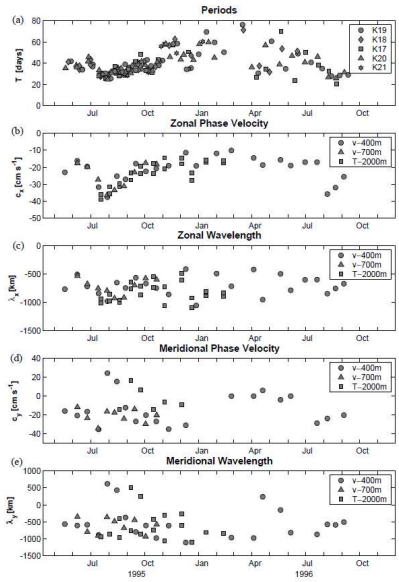

1. Mode barokline Rossbywelle

$$\omega = \frac{-\beta k_x}{k_x^2 + k_y^2 + f^2/c_1^2},$$

Brandt et al., 2002

Somalistrom Wellenausbreitung

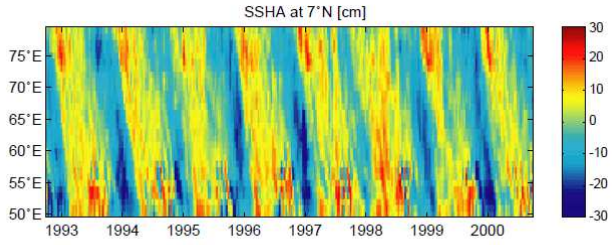

Fig. 2. Longitude–time plot of TOPEX/POSEIDON SSHA at 7°N.

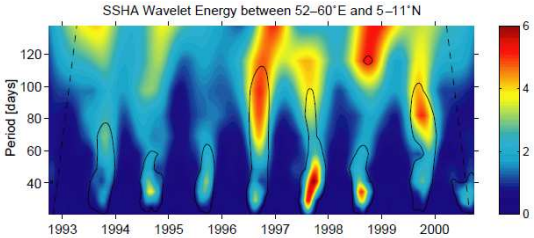

Fig. 4. Period–time plot of normalized SSHA wavelet energy averaged between 52–60°E and 5–11°N. Solid lines mark the 95% significance level.

Brandt et al., 2002

Wyrtki Jet

Oberflächen-
strömung

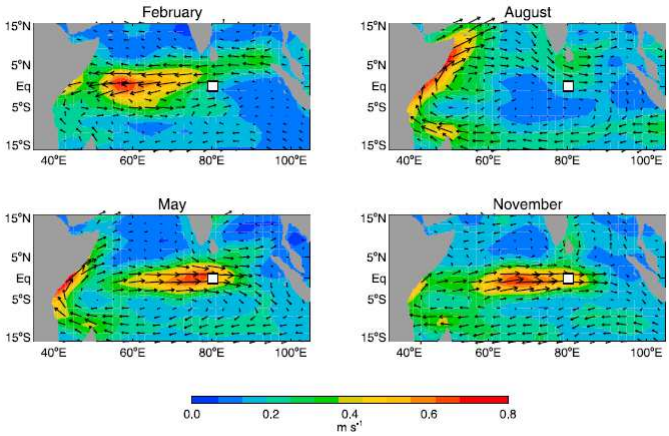

Figure 1. Monthly climatologies of surface velocity (vectors) and scalar speed (color shading) from ship drift observations for February, May, August, and November [*Cutler and Swallow*, 1984]. The white box at 0°, 80.5°E indicates the position of RAMA ADCP observations.

Nagura & McPhaden, 2010

Equatorial Jet (Wyrtki Jet)

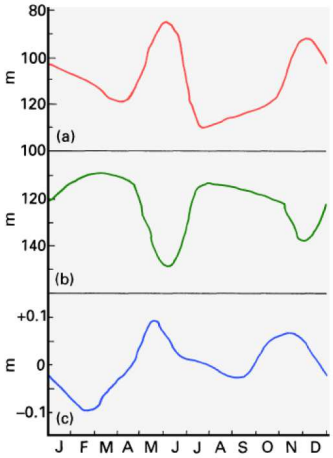

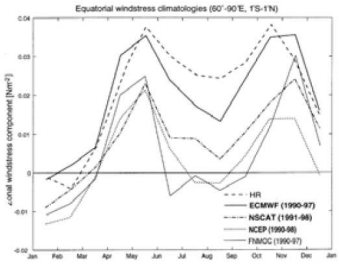

Fig. 11.6. Climatological mean monthly thermocline depth and sea level at the equator.

(a) Depth of 20°C isotherm off Africa,

(b) depth of 20°C isotherm off Sumatra,

(c) sea level at the west coast of Sumatra. After Wyrtki (1973a)

Equatorial Jet (Wyrtki Jet)

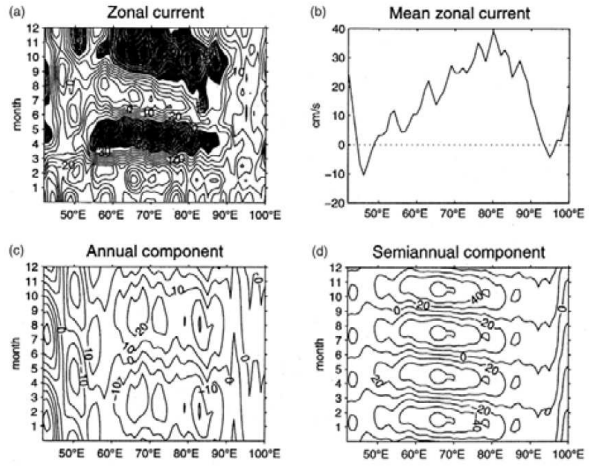

Fig. 21. Longitude-time plots of zonal currents in the 1°S–1°N latitude band, showing the a) total current; and its b) annual-mean; c) annual; and d) semiannual components. (After Han et al., 1999.)

Schott & McCreary, 2001

Wyrtki Jet

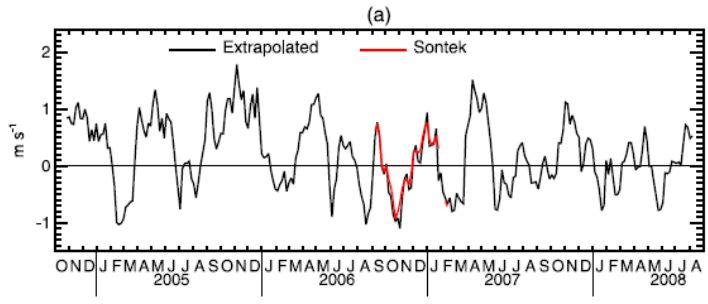

Zonale Strömung bei 80° 30‘ E

Nagura & McPhaden, 2010

Wyrtki Jet

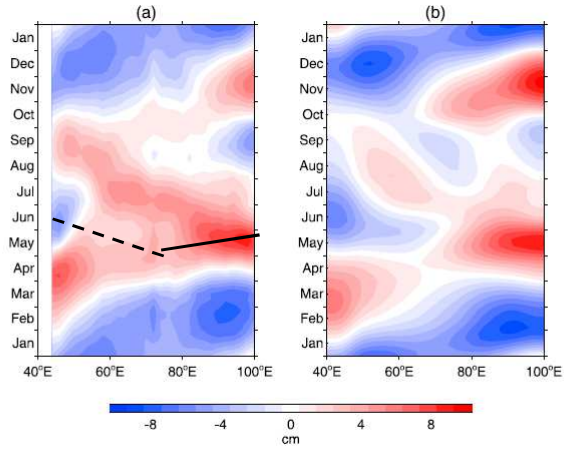

Figure 12. Climatological mean seasonal cycles of SSH along the equator for (a) the observations and (b) the K-R1 model. Record length means are subtracted so that the modeled SSH can be compared with the observed SSH. Climatologies are based on weekly data smoothed with a 35 day running mean filter.

Meerespiegelhöhe

Propagation von äquatorialen Kelvin und Rossbywellen

Nagura & McPhaden, 2010

Competing theories

Lighthill 1969: remote forcing through equatorial waves, response after 4 weeks

Cox 1970: local forcing through coastal winds, response time 2 weeks

Anderson and Rowlands 1976: combined effects of local and remote forcing, stacked response

Anderson and Moore 1979: inertial overshoot rapid response

Seasonal Somali Current

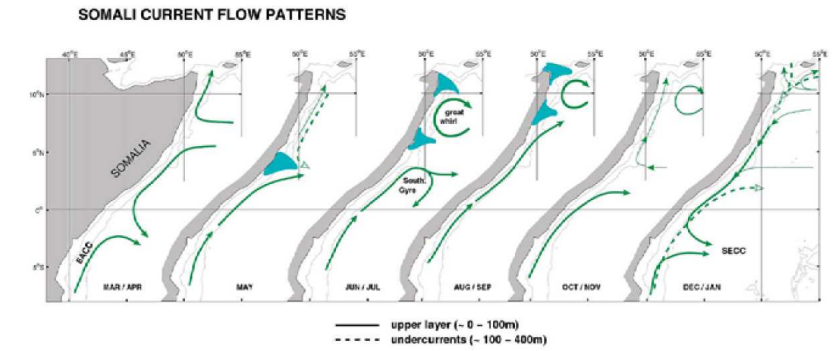

Fig. 32. Schematic diagram of the Somali Current upper-layer flow patterns over the course of the year. Also marked are undercurrents as presently known (after Schott et al., 1990, with revisions). See Figs. 8, 9 and Appendix for acronyms and text for details.

Schott & McCreary, 2001

Süd Java Strom

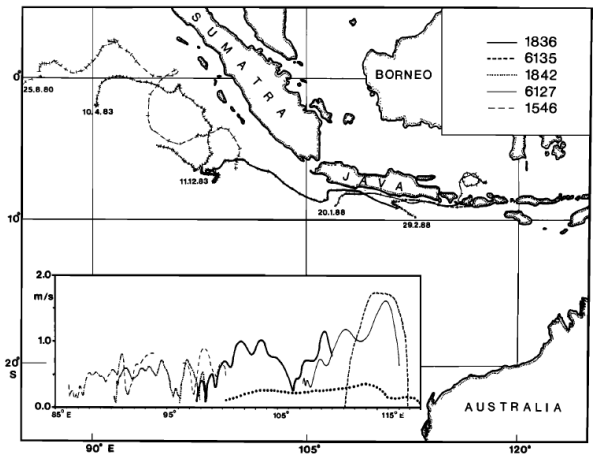

Fig. 1. Trajectories of satellite tracked drifters in the South Java Current. Tick marks indicate the start of successive UTC days. The inset shows mean current speeds of drifters versus longitude; the dotted line is mean alongshore current speed from shipdrifts during the NE monsoon (November-February).

Umwandlung der äquatorialen Kelvin Welle in zwei Küsten-Kelvinwellen

Driftertrajektorien

Quadfasel & Cresswell, 1992

Süd Java Strom

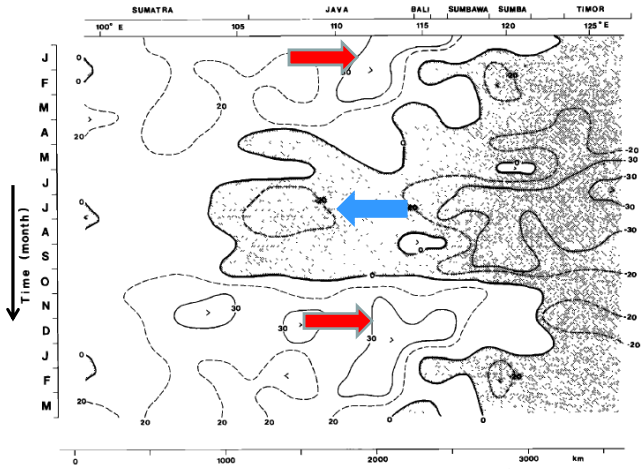

Fig. 2. Time-latitude diagram of alongshore surface current speed (centimeters per second) in the South Java Current based on 1° square monthly averages of shipdrifts [KNMI, 1949]. The stippled area indicates westward flow.

Oberflächen-strömungen

Überlagerung von saisonalen windgetriebenen geostrophischen Strömungen und Küsten-Kelvin-Wellen

Surface circulation Bay of Bengal

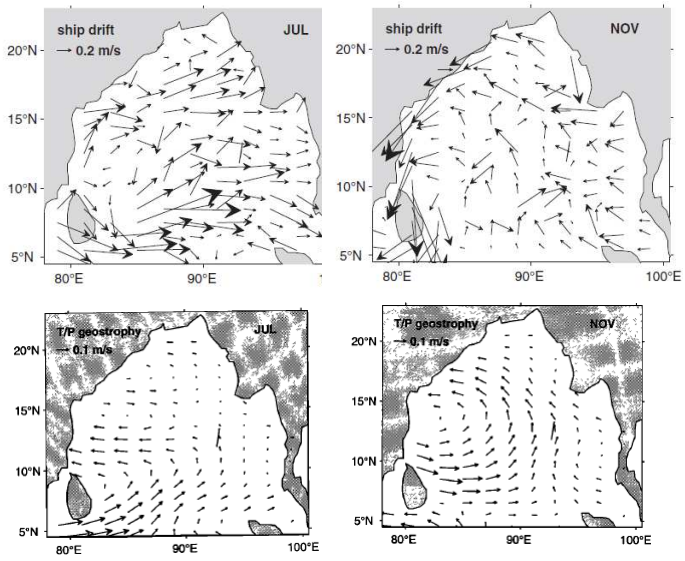

Lokale Sverdrup Zirkulation plus Einflüsse von Küsten-Kelvinwellen

Eigenheer & Quadfasel, 2000

Indonesian Archipelago

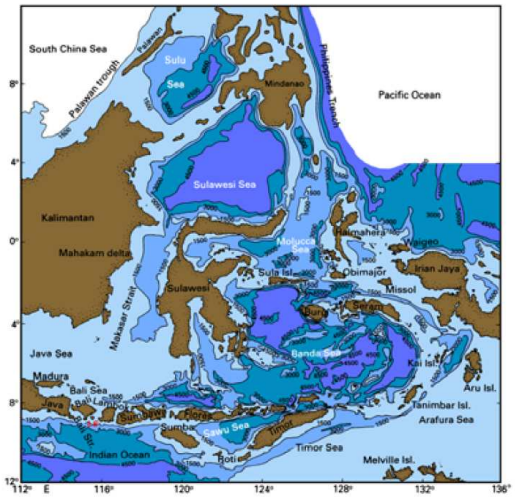

Fig. 13.5. Topography of the Australasian Mediterranean Sea. Depths are in m. LS: Lombok Strait.

Tomczak & Godfrey, 2005

Indo-Pacific (Indonesian) Throughflow

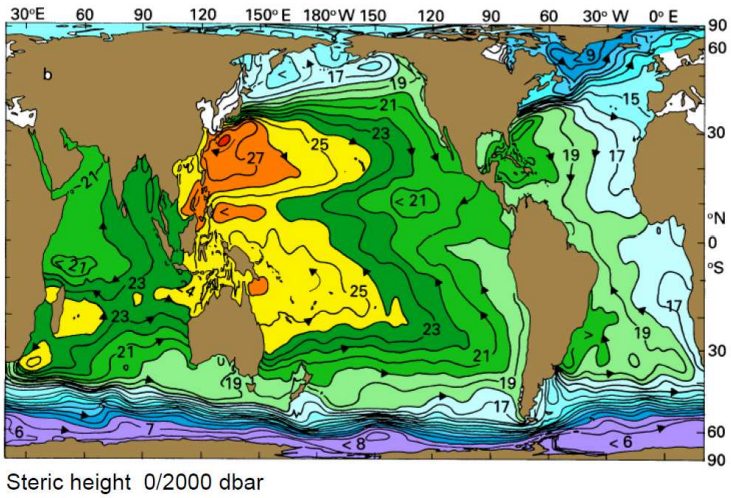

Steric height 0/2000 dbar

Tomczak & Godfrey, 2005

Indo-Pacific (Indonesian) Throughflow

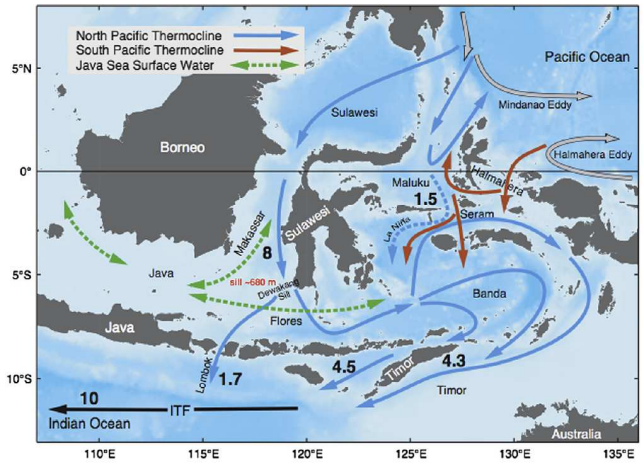

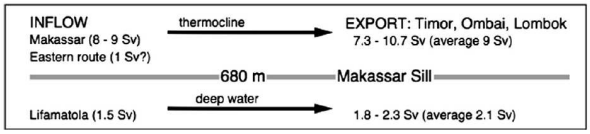

Leeuwin Current

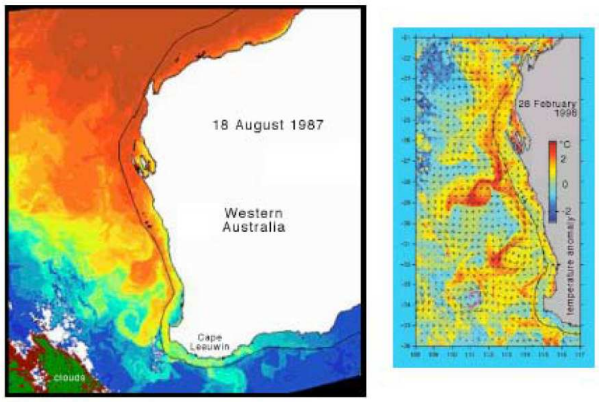

Fig. 11.21. Satellite images of sea surface temperature in the Leeuwin Current and associated eddies. Warm is red, cold is blue. Left: Sea surface temperature in August 1987. The Leeuwin Current is seen as a band of warm water along the western coastline that continues around Cape Leeuwin. The black line indicates the shelf break. (b) Sea surface temperature anomalies (departures from the latitudinal mean temperature) in February 1996 showing large eddies near Cape Leeuwin. Black arrows indicate surface currents. © CSIRO Marine Research, reproduced by permission.

Tomczak & Godfrey, 2005

Leeuwin Current

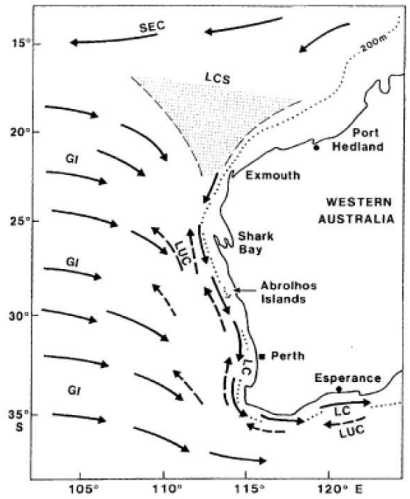

Schott & McCreary, 2001

Fig. 52. Schematic diagram showing the Leeuwin Current (LC) off western Australia, the geostrophic inflow from the west (GI), the Leeuwin Undercurrent offshore (LUC) and the presumed Leewin Current source area (LCS). (From Pearce, 1991.)

Leeuwin Current

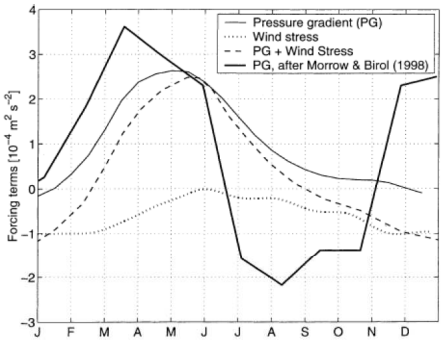

Fig. 54. Annual cycle of forcing terms off western Australia, showing meridional pressure gradient from climatological hydrographic data (PG, thin solid) and wind stress (dotted), as well as their sum (dashed; after Godfrey & Ridgeway, 1985) and new evaluations of pressure gradient from T/P altimetry (heavy solid) by Morrow and Birol (1998). Note the strong semiannual component in the latter curve.

Schott & McCreary, 2001

‘Unusual’ current systems

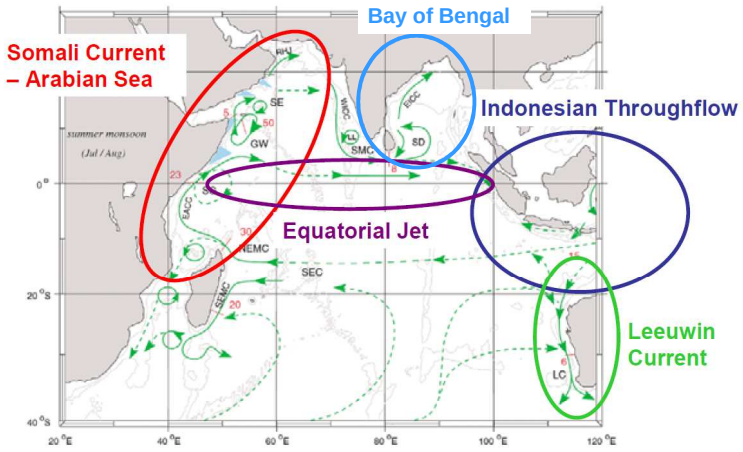

Fig. 8. A schematic representation of identified current branches during the Southwest Monsoon, including some choke point transport numbers ($Sv=10^6 m^3 s^{-1}$). Current branches indicated (see also Fig. 9) are the South Equatorial Current (SEC), South Equatorial Countercurrent (SECC), Northeast and Southeast Madagascar Current (NEMC and SEMC), East African Coast Current (EACC), Somali Current (SC), Southern Gyre (SG) and Great Whirl (GW) and associated upwelling wedges, Socotra Eddy (SE), Ras al Hadd Jet (RHJ) and upwelling wedges off Oman, West Indian Coast Current (WICC), Laccadive High and Low (LH and LL), East Indian Coast Current (EICC), Southwest and Northeast Monsoon Current (SMC and NMC), South Java Current (JC) and Leeuwin Current (LC). See text for details.

Schott & McCreary, 2001

Near surface circulation SW-Monsoon

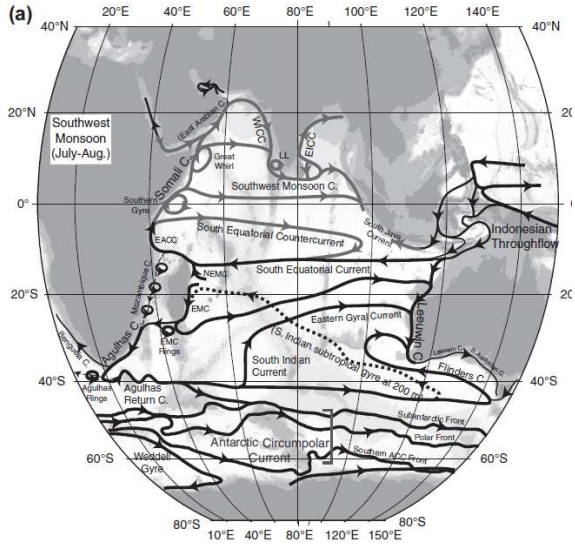

Talley at al., 2011

Agulhas Current

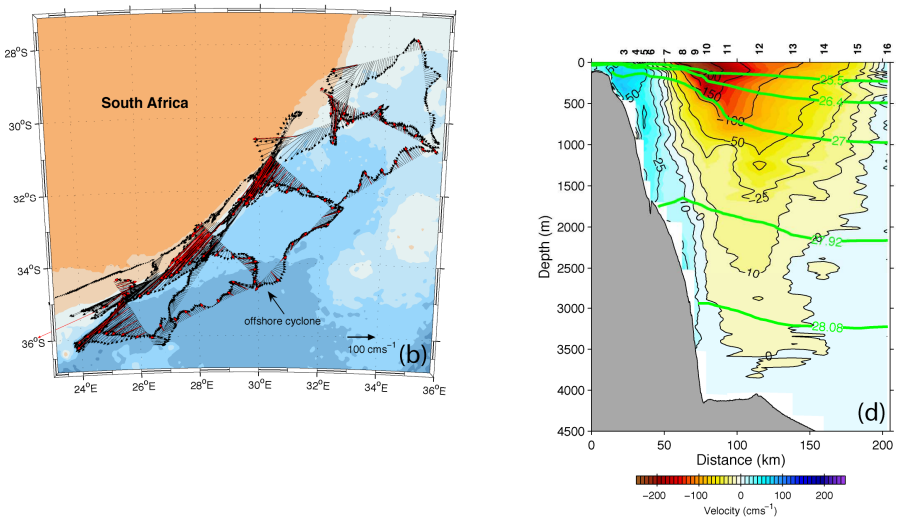

Beal et al, 2006

Agulhas Current

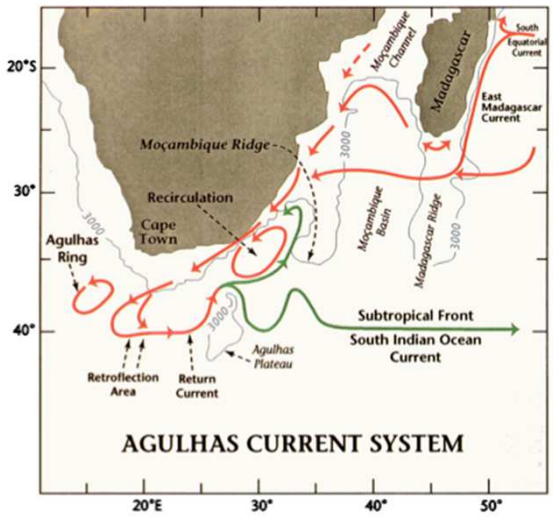

Schmitz, 1995

Agulhas

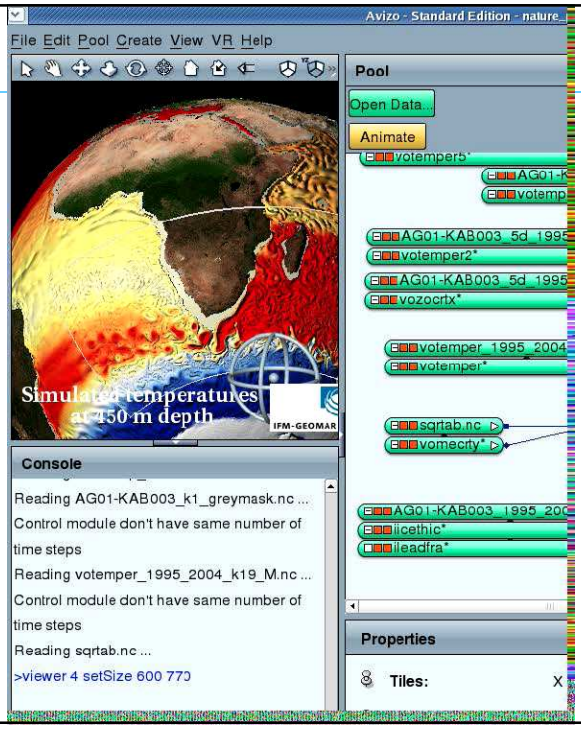

Great Ocean Conveyor – warm water route

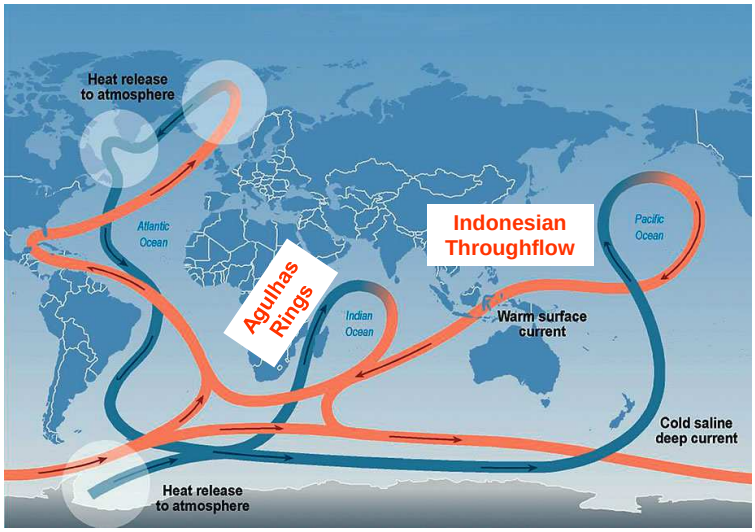

ORCA

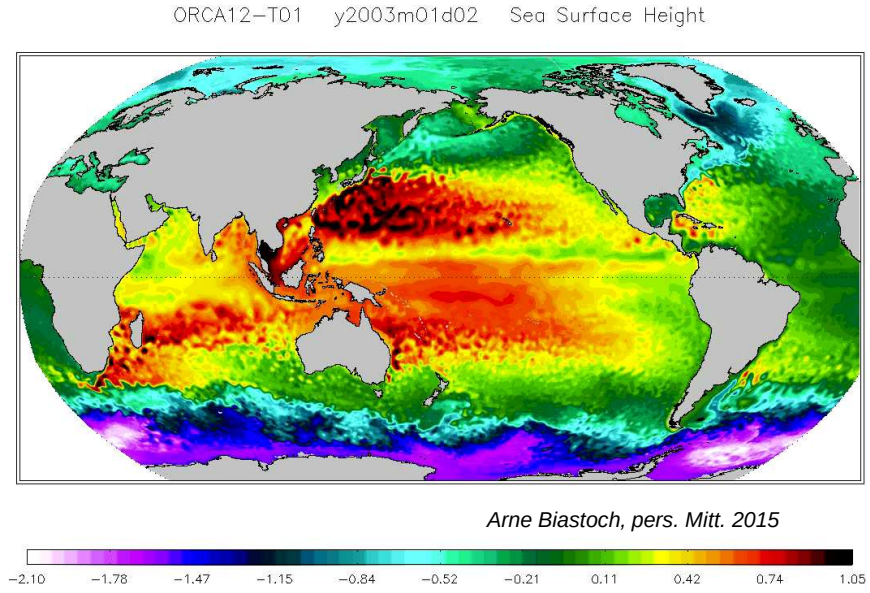

Arne Biastoch, pers. Mitt. 2015